Enhanced Spatio-Temporal Resolution using Dynamic Sparse Coding for EEG Inverse Problem Solutions

J.D. Martinez-Vargas, E. Giraldo, and G. Castellanos-Dominguez

***Abstract*—We introduce a novel approach to source reconstruction from electroencephalographic (EEG) recordings, introducing physiologically motivated spatio-temporal constraints over the source representation. Within a Dynamic Sparse Coding (DSC) formulation, we promote the source reconstruction to encode the strong temporal dynamics of EEG data, enabling the analysis of smooth and localized characteristics in space. Consequently, by adjusting the ratio between a couple of included regularization terms, our method enables reaching a trade-off between temporal and spatial resolution, which can be ruled depending on each specific analysis and provided data. We validate the method performance on simulated event-related potentials, fixing a distinct number of active sources and under different values of signal-to-noise ratio. Also, testing is performed on real-world EEG data related to emotion brain activity, for which the obtained results prove that the most active sources originate in cortical areas related to visual and attention processes, as well as in regions involved in emotional processing. Additional comparison with the state-of-the-art methods is also performed for simulated and real EEG signals. As a result, the proposed DSC based solution enhances the EEG characterization of source activity, particularly, when dealing with strong temporal dynamics.**

***Index Terms*—EEG, inverse problem, Dynamic Sparse Coding, Fused Lasso, Spatio-Temporal Constraints, Emotion classification.**

I. Introduction

In the recent past, *electroencephalography* (EEG) has been increasingly employed as a non-invasive technique in understanding the brain functions and neural dynamics in humans, mainly, because of the following reasons: *i*) The ease of manipulation at a low implementation cost, *ii*) The ability to measure real-time responses directly from the neural activity without delays [1], *iii*) The high temporal resolution that allows investigating many different kinds of dynamic brain activation during multiple cognitive tasks [2]. Particularly, EEG analysis is a valuable tool for studying the brain functionality and interaction patterns of neural activity across space, time, and frequency [3], [4], [5], [6].

Manuscript received September 26, 2018; revised May 23, 2019. This work was carried out under the funding of the Departamento Administrativo Nacional de Ciencia, Tecnología e Innovación (Colciencias). Research project: 111077757982 "Sistema de identificación de fuentes epileptogénicas basado en medidas de conectividad funcional usando registros electroencefalográficos e imágenes de resonancia magnética en pacientes con epilepsia refractaria: apoyo a la cirugía resectiva".

J.D Martínez-Vargas is with the Instituto Tecnológico Metropolitano, Medellín, Colombia, e-mail: juanmartinez@itm.edu.co

E. Giraldo is with the Department of Electrical Engineering, Universidad Tecnológica de Pereira, Pereira, Colombia, e-mail: egiraldos@utp.edu.co.

G. Castellanos-Dominguez is with the Signal Processing and Recognition Group, Universidad Nacional de Colombia sede Manizales, Manizales, Colombia, e-mail: fmgrisalesf@unal.edu.co

In the brain functional analysis, a challenging task (termed *Electromagnetic Source Imaging* - ESI) is to determine the foci of activated neural populations (or sources) and evoked time courses in the brain cortex, giving rise to a scalp potential recording [7]. However, ESI is an ill-posed temporal inverse problem, i.e., a map with regional activation does not readily permit inferences about when and in which order these activation have occurred since a single EEG recording can be explained by an infinite number of different ESI solutions [8]. To overcome the ill-posed property, the solution to the EEG inverse problem holds a set of additional constraints that are based, mainly, on prior information about the dipole distribution, being the Distributed Source Solutions widely used in which several dipole sources (with fixed locations and possibly fixed orientations) are distributed across the whole brain volume or cortical surface [9]. To this end, a regularized solution can be applied that approximates an ill-posed task by a family of neighboring well-posed problems, using the regularization terms to incorporate some prior information.

A straightforward regularized approach is the Tikhonov regularization that searches for the solution with minimum power (like in Minimum norm estimates [10]), but producing a very poor estimation of the actual source locations. To improve localization accuracy, the depth-compensated inverse solution is performed under the constraint of smoothly distributed sources (like in Low-resolution electrical tomography or Standardized low-resolution brain electromagnetic tomography [11]). Nevertheless, these methods tend to overestimate the location of active areas and do not reflect the assumption stating that only a few brain regions can be active when a brain neurological process takes place [12]. With the aim to estimate the focal source activation more accurately, several regularized regressions have been proposed in the form of the Multiple Penalized Least Squares Model that includes the use of non-convex penalty functions, leading to sparse representations that have been regarded as more likely to be separable in describing smooth localized patches of potentially active regions [13]. Within the Bayesian framework, these patches can be modeled by a set of covariance priors like in *Multiple Sparse Priors* (MSP) [14] or by expanding the current density into a sparse combination of spatial basis fields like in *Sparse Basis Field Expansions* (S-FLEX) [15]. However, there is no temporal assumption about the neural activity dynamics even that either solution provides a coherent spatial structure [16], [17]. To resolve this issue, the spatial and temporal patterns of neural activity must be further incorporated, considering that a small number of events (confined in space and/or time) generates each measured scalp potential signal. Thus, the

authors in [18] make use of both spatial and temporal bases to span the local regions of cortex within specific frequency bands and/or time windows, enabling to better determine where and when a significant activity occurs. A detailed analysis by using frequency bands is also performed in [19].

Besides fostering a physiologically motivated spatial structure, prior information has also been included in the form of temporal constraints. To this end, some solutions previously decompose the EEG space/time data into a small number of components (or atoms), encoding the spatial and temporal patterns for the inverse problem solution as in [20], [21]. However, these methods are statistically sub-optimal due to the extraction of relevant atoms and ESI must be carried out simultaneously [22]. In other approaches, time-frequency representations are used to provide insightful information about the dynamics of neural processes [23]. Still, they demand manual tuning of the regularization parameters [24]. The combination of spatial and temporal constraints are also contemplated by formulating the ESI problem through state-space models [25]. But, these methods do not lead to an adequate focal neural activity estimate [26]. Consequently, the spatially in-homogeneous temporal evolution must be developed for accurately reconstructing the focal brain activity with strong temporal dynamics.

In this work, we introduce a spatio-temporal ESI solution that promotes the spatial sparsity to reconstruct the focal neural activity and temporal homogeneity. With the goal of following the strong temporal dynamics accurately, the spatio-temporal decomposition of source activation comprises the next three stages: *i*) A predefined dictionary of spatial basis fields to encourage neurophysiologically motivated structure in the space domain, namely, spatial in homogeneity, *ii*) Estimation of the matrix of spatio-temporal coefficients, and *iii*) a constraint set that promotes the desired properties of the spatio-temporal coefficients. We incorporate these constraints within a *Dynamic Sparse Coding* (DSC) framework that enables dealing with high volumes of data having sparse and time-varying patterns. Hence, DSC allows reconstructing the time courses related to potentially non-stationary source activation with focal spatial patterns. Moreover, by seeking the sparse structure through a weighted combination of spatial and temporal penalty terms, we rule a trade-off between spatial locality and temporal homogeneity quantified by a single hyperparameter. Lastly, we show that DSC model can be readily extended as an EEG Source Connectivity approach, aiming to enhance the estimation of interactions between distant brain areas. This manuscript is organized as follows: In Section II, we give an introduction to the ESI methods and present our proposal DSC solution. In Section III, we assess the DSC reconstruction quality of a simulated ERP activity and compare its performance against state-of-the-art methods, namely MSP and S-FLEX methods, encouraging focal solutions. Validation is also achieved for real emotional EEG data, incorporating a source connectivity analysis. In Sections IV and V, we address the interpretation of the obtained results, highlighting their contributions in Section VI.

II. Methods

A. EEG inverse problem

With the aim of representing the electromagnetic field magnitude measured at the scalp, we assume the following linear model [27]:

$$\boldsymbol{Y} = \boldsymbol{L}\boldsymbol{J} + \boldsymbol{\Xi}, \tag{1}$$

where $\boldsymbol{Y}\in\mathbb{R}^{C\times T}$ is the EEG data collected by $C\in\mathbb{N}$ sensors at $T\in\mathbb{N}$ time samples, $\boldsymbol{J}\in\mathbb{R}^{D\times T}$ is the amplitude of $D\in\mathbb{N}$ current dipoles (or sources), which are distributed throughout the cortical surface with a fixed orientation perpendicular to it, and $\boldsymbol{L}\in\mathbb{R}^{C\times D}$ is the gain matrix (termed *lead field matrix*), relating the source strengths to the measured EEG data. Also, the effect of noise on the brain activity measured by EEG recordings is modeled by the error matrix $\boldsymbol{\Xi}\in\mathbb{R}^{C\times T}$, so that the uncorrelated noise is assumed to be a Gaussian-distributed random process with zero mean and covariance matrix $\boldsymbol{Q}_{\boldsymbol{\Xi}}\in\mathbb{R}^{C\times C}$.

Although there are several distributed inverse solutions to estimate the source amplitude $\boldsymbol{J}$, we rely on a generalized problem formulation, termed *Multiple Penalized Least Squares Model*, that includes the following minimization cost function [13]:

$$\widehat{\boldsymbol{J}} = \underset{\boldsymbol{J}}{\operatorname{argmin}}\{||\boldsymbol{Y}-\boldsymbol{L}\boldsymbol{J}||_F^2 + \sum_{m\in M}\lambda_m\Theta_m(\boldsymbol{J})\}, \tag{2}$$

where $\{\lambda_m\in\mathbb{R}^+\}$ is the regularization parameter set and $\{\Theta_m(\boldsymbol{J})\in\mathbb{R}\}$ is the introduced penalty function set. Note that the first quadratic term in Eq. (2) is the log-likelihood (notation $||\cdot||_F$ stands for the Frobenius norm), while the second term holds all prior information encoded in $M\in\mathbb{N}$ regularized penalty functions.

B. Sparsity and temporal homogeneity constraints using dynamic sparse coding

As a rule, by promoting more focal solutions together with smooth current distributions, the inverse problem formulations tend to provide a better source reconstruction than other solutions that are either purely smoothed or grounded only on sparse representations [28]. Therefore, the current density can be formulated by a linear combination of $S\in\mathbb{N}$ spatial basis functions $\boldsymbol{\Phi}\in\mathbb{R}^{D\times S}$, which are both locally smooth and spatially limited, as described below:

$$\boldsymbol{J} = \boldsymbol{\Phi}\boldsymbol{H}, \tag{3}$$

where $\boldsymbol{H}\in\mathbb{R}^{S\times T}$ are the weights introduced to reflect the desired properties of spatial basis sets. Thus, each column of $\boldsymbol{H}$ draws a single distributed pattern with compact spatial support.

As discussed in [29], the spatial extent of a source prior can be extracted from the smoothing operator that employs the Green function, $\boldsymbol{\mathcal{G}}=\exp\{\sigma\boldsymbol{\Lambda}\}$, representing the inverse of a (sufficiently regular) linear differential operator. So, the matrix $\boldsymbol{\Lambda}\in\mathbb{R}[0,1]^{D\times D}$ encodes all neighborhood relationships between the cortical mesh nodes, which belong to the solution space that is bounded by the area covering the active regions $\sigma\in\mathbb{R}^+$ [30].

Besides, we model the non-stationary source activations by enforcing a temporary structure of the weight matrix $\boldsymbol{H}$ through the use of short-time windows. Therefore, we incorporate a couple of constraints (one spatial and another

temporal) into the following regularized penalty function, termed *Dynamic Sparse Coding – DSC*:

$$\Theta(\boldsymbol{J};\lambda_s,\lambda_t)=\lambda_s||\boldsymbol{H}||_1+\lambda_t\sum_{t\in T-1}||\boldsymbol{h}_{t+1}-\boldsymbol{h}_t||_1 \quad (4)$$

where $\lambda_s\in\mathbb{R}^+$ and $\lambda_t\in\mathbb{R}^+$ are the spatial and temporal regularization parameters, respectively, and $\boldsymbol{h}_t\in\mathbb{R}^{C\times 1}$ is t-th column vector that holds the temporary structure of $\boldsymbol{H}$. Notation $||\cdot||_p$ stands for the L_p-norm.

Based on Eq. (4), the above objective function in Eq. (2) comes in the following generalized form:

$$\widehat{\boldsymbol{H}}=\underset{\boldsymbol{H}}{\operatorname{argmin}}\{||\boldsymbol{Y}-\boldsymbol{L}\boldsymbol{\Phi}\boldsymbol{H}||_F^2 + \lambda_s||\boldsymbol{H}||_1+\lambda_t\sum_{t\in T-1}||\boldsymbol{h}_{t+1}-\boldsymbol{h}_t||_1\}, \quad (5)$$

Hence, the estimation of the neural activity in Eq. (3) is rewritten as follows:

$$\boldsymbol{J}=\boldsymbol{\Phi}\widehat{\boldsymbol{H}} \quad (6)$$

Note that sparseness is encouraged by the first penalty term in Eq. (5) that assigns a high cost to the matrices with large absolute values, and thus effectively shrinking all elements towards to zero. This situation means that just a few spatial dictionary bases will explain the main brain activity. In turn, the second term encourages the temporal homogeneity by penalizing the difference between consecutive time points, yielding a smooth solution over time.

C. DSC Optimization under regularized penalty functions

Even that the DSC optimization task is convex, it is a high-dimensional and large-scale problem, being not trivial to optimize because the non-smooth penalty function intended in Eq. (4). Hence, we reformulate the non-smooth penalty term in the form of the smooth proximal gradient algorithm that allows rewriting the fusion penalty term through an introduced vertex-edge incident matrix $\boldsymbol{P}\in\mathbb{R}^{T\times(T-1)}$, so that we encode the signal structure as below [31]:

$$\lambda_t\sum_{t\in T-1}||\boldsymbol{h}_{t+1}-\boldsymbol{h}_t||_1=\lambda_t||\boldsymbol{H}\boldsymbol{P}||_1.$$

In order to calculate the smooth proximal gradient, we rewrite the overall penalty, relying on the fact that the dual norm of the entry-wise matrix L_∞ coincides with L_1 norm, yielding the following penalty function:

$$||\boldsymbol{H}\widetilde{\boldsymbol{P}}||_1\equiv\underset{||\boldsymbol{A}||_\infty\leq 1}{\operatorname{argmax}}\langle\boldsymbol{A},\boldsymbol{H}\widetilde{\boldsymbol{P}}\rangle, \quad (7)$$

where $\boldsymbol{A}\in\mathbb{R}^{S\times(T-1)}$ is a some auxiliary matrix associated with $||\boldsymbol{H}\widetilde{\boldsymbol{P}}||_1$. Notations $\langle\cdot\rangle$ and $\|\cdot\|_\infty$ stand for the matrix inner product and matrix entry-wise L_∞ norm (that is, the maximum absolute value of all matrix entries), respectively. It is worth noting that the temporal regularization parameter λ_t is now included into the term $||\boldsymbol{H}\widetilde{\boldsymbol{P}}||_1$ by making $\lambda_t||\boldsymbol{H}\boldsymbol{P}||_1=||\boldsymbol{H}\lambda_t\boldsymbol{P}||_1$, where $\widetilde{\boldsymbol{P}}=\lambda_t\boldsymbol{P}$.

So far, the penalty formulation in Eq. (7) does not enable a function that is just smooth enough over $\boldsymbol{H}$. To cope with this issue, we propose to encourage the approximation of Eq. (4) to be sufficiently smooth by introducing the following auxiliary function that is strongly convex [32]:

$$f_\mu(\boldsymbol{H})=\underset{||\boldsymbol{A}||_\infty\leq 1}{\operatorname{argmax}}\{\langle\boldsymbol{A},\boldsymbol{H}\widetilde{\boldsymbol{P}}\rangle-\mu d(\boldsymbol{A})\} \quad (8)$$

where $\mu\in\mathbb{R}^+$ is a smoothing parameter and $d(\boldsymbol{A})\equiv\frac{1}{2}\|\boldsymbol{A}\|_F^2$ is an arbitrary smooth strong-convex function. From the Nestrov's theorem, it follows that $f_\mu(\boldsymbol{H})$ is convex and continuously differentiable in $\boldsymbol{H}$, i.e., $f_\mu(\boldsymbol{H})$ is smooth and $\nabla f_\mu(\boldsymbol{H})$ is Lipchitz continuous, so that the gradient of $f_\mu(\boldsymbol{H})$ in $\boldsymbol{H}$ takes the following form [33]:

$$\nabla f_\mu(\boldsymbol{H})=\widehat{\boldsymbol{A}}\,\widetilde{\boldsymbol{P}}^\top \quad (9)$$

where $\widehat{\boldsymbol{A}}=\mathcal{S}\{\boldsymbol{H}\widetilde{\boldsymbol{P}}/\mu\}$ is the optimal solution for $\boldsymbol{A}$ obtained in Eq. (8), and $\mathcal{S}\{\cdot\}$ is the shrinkage operator that is defined for each entry $\xi\in\mathbb{R}$ as:

$$\mathcal{S}\{\xi\}=\begin{cases}\xi, & |\xi|<1\\ \operatorname{sgn}(\xi), & \text{otherwise}\end{cases}$$

Lastly, provided in terms of the smoothing approximation $f_\mu(\boldsymbol{H})$, the minimization DSC problem results in the next smooth optimization framework:

$$\begin{aligned}\widehat{\boldsymbol{H}}&=\underset{\boldsymbol{H}}{\operatorname{argmin}}\{||\boldsymbol{Y}-\boldsymbol{L}\boldsymbol{\Phi}\boldsymbol{H}||_F^2+\lambda_s||\boldsymbol{H}||_1+f_\mu(\boldsymbol{H})\}\\&=\underset{\boldsymbol{H}}{\operatorname{argmin}}\{\tilde{f}(\boldsymbol{H})+\lambda_s||\boldsymbol{H}||_1\}\end{aligned} \quad (10)$$

where $\tilde{f}(\boldsymbol{H})=||\boldsymbol{Y}-\boldsymbol{L}\boldsymbol{\Phi}\boldsymbol{H}||_F^2+f_\mu(\boldsymbol{H})$ is the smooth term, for which the gradient in Eq. (9) is defined as below:

$$\nabla\tilde{f}(\boldsymbol{H})=(\boldsymbol{L}\boldsymbol{\Phi})^\top(\boldsymbol{L}\boldsymbol{\Phi}\boldsymbol{H}-\boldsymbol{Y})+\widehat{\boldsymbol{A}}\,\widetilde{\boldsymbol{P}}^\top \quad (11)$$

Expressed by the smooth function in Eq. (4), therefore, the initial DSC optimization task is now recast as the smoothed optimization version in Eqs. (10) and (11) that we implement, employing the Fast Iterative Shrinkage-Thresholding Algorithm (FISTA) [31].

III. Experimental set-up

A. Models of spatio-temporal sparseness

In order to validate the improvement in spatio-temporal resolution that is contributed by the inverse problem framework, the proposed solution using Dynamic Sparse Coding is tested on synthetic and real-world datasets of EEG signals. For this purpose, the performance validation is verified by comparing with two baseline EEG inverse solutions, namely, MSP and S-FLEX. Also, we study the following DSC ratios for the regularization parameters: λ_s: λ_t=90:0 (termed LASSO), 90:30, 90:90, 30:90, 0:90 (termed FUSION). The test range is selected to investigate to what extent the DSC solution enables a compromise between the LASSO solution (that is, solely space regularization) and FUSION (the entirely time reconstruction).

Fig. 1 illustrates the sparseness patterns estimated for the tested inverse methods, so that each time-space representation is computed for a single EEG recording measured by 32 electrodes, assuming 60 sources and simulating a random lead field matrix. As seen in Fig. 1(c) (patterns produced by MSP) and Fig. 1(b) (S-FLEX), either solution promotes just sparseness of the spatial patterns and cannot rightly group the sources along the time domain,

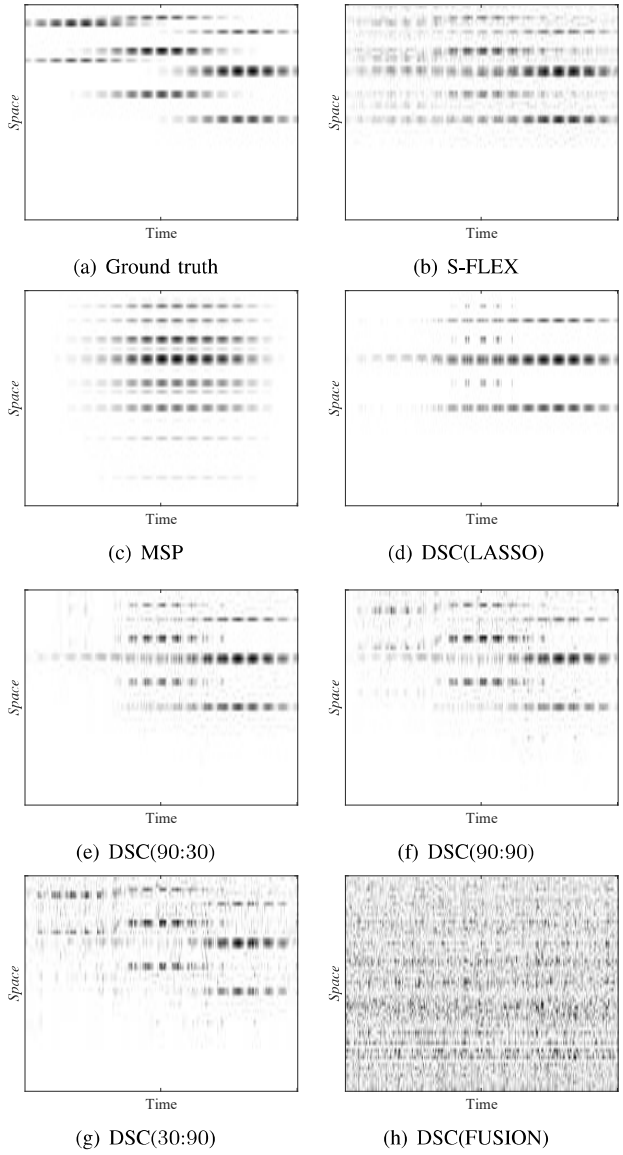

(a) Ground truth (b) S-FLEX

(c) MSP (d) DSC(LASSO)

(e) DSC(90:30) (f) DSC(90:90)

(g) DSC(30:90) (h) DSC(FUSION)

Fig. 1. Time-space representation models of reconstructed activity performed by the EEG inverse problem solutions tested in this work.

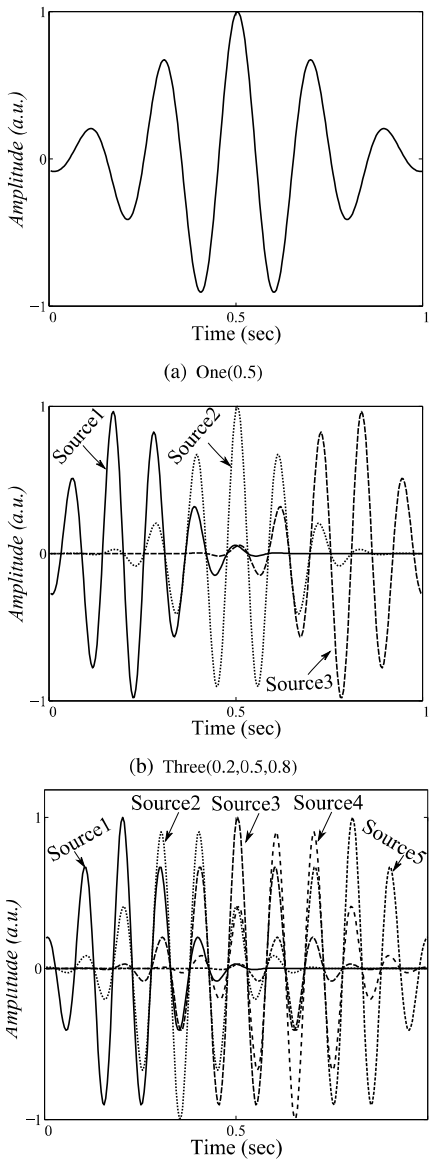

(a) One(0.5)

(b) Three(0.2,0.5,0.8)

(c) Five(0.2,0.35,0.5,0.65,0.8)

Fig. 2. Examples of the simulated sources for one, three, and five active dipoles showing the mean values fixed for each case of the simulated Morlet wavelets.

resulting in an inaccurate temporal source reconstruction as compared to the simulated ground truth (see Fig. 1(a)). A similar situation holds for the LASSO solution when having only the spatial regularization as shown in Fig. 1(d).

On the other hand, the inclusion of sparseness constraints in both domains makes each DSC solution be a more accurate spatio-temporal resolution. Nevertheless, the quality of EEG reconstruction depends on the fixed regularization ratio. Thus, if the spatial regularization parameter is higher than the temporal one ($\lambda_s > \lambda_t$), the performed reconstruction is spatially enhanced even that some temporal patterns may be missed as noted in Fig. 1(e). By contrast, if we make $\lambda_s \leq \lambda_t$, the temporal structure of reconstructed sources tends to be closer to the original EEG simulation, but some blurred sources can appear in the spatial domain (see Figs. 1(f) and 1(g)). Moreover, the insertion of the purely temporal constraint by DSC (that is, FUSION) does not decode any spatio-temporal information of the reconstructed activity (Fig. 1(h)). Apparently, the lack of spatial resolution degrades the temporal activity decoding.

B. Simulated EEG data

The most common approach to assessing the EEG inverse solution is the validation performed on specially designed EEG sets, for which the brain activity is already known so that the estimation quality can be objectively verified. So, we create 128-channel EEG data (noted as `SD-1`), reproducing the pseudo-EEG at the positions defined by the extended international BIOSEMI system. Here, we generate the non-stationary EEG activity of active dipoles using a signal set produced by a real Morlet wavelet that lasts one-second long, sampled at $250\,Hz$, and having the following parameters:

- Random central frequency with a mean of $9\,Hz$ and standard deviation of $2\,Hz$, sampled from a Gaussian distribution.
- Random time shift generated by the normal distribution with a standard deviation of $0.05\,s$ and mean value selected as shown in Fig. 2.
- The activity is simulated for the cases of one, three,

and five active dipoles, fixing their location randomly from trial to trial.

Besides, the simulated time courses are assigned to the adjacent nodes distributed on the computed cortical mesh that is centered at the fixed random location, yielding the known activity $\boldsymbol{J}$. Then, the simulated source activity is mapped to EEG sensor space through a realistic volume conductor model of the human head that is obtained from a tessellated surface in the gray-white matter interface with $D{=}8196$ vertices (i.e., the number of available source locations), having the source orientations fixed orthogonally to the surface. Also, the lead fields are computed using a standardized volume conductor model (specifically, we employ the boundary element method) with a mean distance between neighboring vertices adjusted to $5\,mm$.

With the aim to test the influence of the non-stationary brain activity on the neural reconstruction performance, we alter the noise conditions of EEG data. Namely, we add the measurement noise to obtain the following experimental values of *Signal-to-Noise Ratio* (SNR): $-5, 0, 10$, and $15\,dB$. As a result, a testing set holding 30 trials for every SNR value and each simulation setting is produced.

Lastly, we reduce the high computational burden of the optimization task in Eq. (1) by using the spatial projector $\boldsymbol{U}$ defined as follows:

$$\widetilde{\boldsymbol{L}} = \boldsymbol{U}^{\top}\boldsymbol{L},$$
$$\widetilde{\boldsymbol{Y}} = \boldsymbol{U}^{\top}\boldsymbol{Y},$$

where $\boldsymbol{U}{\in}\mathbb{R}^{C'\times C}$ holds the C' most significant singular values (spatial modes larger than some tolerance prior given) computed from the lead field matrix. It is important to note that this preprocessing stage, commonly considered for inversion schemes, does not affect the number of sources to be estimated.

Tuning of DSC optimization parameters

In practice, tuning of the constrained optimization framework poses a challenging task, becoming more complicated as the number of parameter increases in the inverse model given in Eq. (5). Thus, a critical issue for solving the Dynamical Sparse Coding solution is the adjustment of the spatial (λ_s) and temporal (λ_t) regularization parameters since their influence affects the quality of neural activity reconstruction the most. To this end, we adjust their ratio, reaching a trade-off between the spatial resolution (provided by LASSO scheme) and the temporal resolution (by FUSION strategy). Like in [28], we fix three different ratios evenly distributed: $\lambda_s/\lambda_t{=}90/30,\ 90/90,\ 30/90$. For the sake of comparison, we also study two more asymptotic values: $\lambda_s{\neq}0$ and $\lambda_t{=}0$ (only spatial regularization) and $\lambda_t{\neq}0$ and $\lambda_t{=}0$ (only temporal regularization).

With the purpose of further simplification, we reduce the searching set of the optimal values using the heuristic approach performed in [34] that fixes λ_s as a fraction of the critical value of $\lambda_{\max}$, i.e., $\lambda_s^{\text{opt}}{=}\beta\lambda_{\max}$, where $\beta{\in}[0,1]$. Thus, if $\beta{=}1$, the source activity $\widehat{\boldsymbol{J}}$ is filled with zeros, meaning that there are no active sources (that is, *the sparsest possible solution*). In the opposite case when $\beta{=}0$, no sparse restriction is imposed. Here, we set $\lambda_{\max}{=}\|\boldsymbol{Y}\|_F$ (data magnitude), and $\beta{=}\alpha/\|\boldsymbol{L}^{\top}\boldsymbol{Y}\|_F$ with $\alpha{\in}[0,1]$. Hence, we use the fixed ratio λ_s/λ_t to get λ_t.

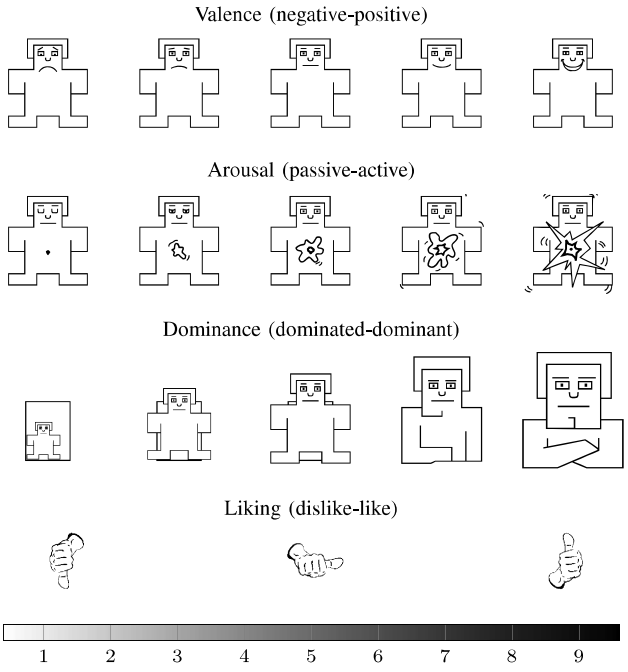

Fig. 3. The Self-assessment manikins scales for valence, arousal, and dominance. The thumbs down/thumbs up symbols are for the liking scale.

Accuracy measures of source reconstruction

The evaluation of tested inverse solutions is achieved regarding the ability to accurately localize and reconstruct the time-courses extracted from the simulated EEG activity. To this end, the localization task is accomplished using the same head model for which the data have been generated. For implementing all solutions, the employed spatial basis $\boldsymbol{\Phi}$ comprises $S{=}512$ elements (256 per hemisphere), which are designed to cover the entire cortical surface.

The accuracy performed by each compared source reconstruction algorithm is assessed for the time and space domains by using the following measures:

Earth-Movers Distance, $\varepsilon_s{\in}\mathbb{R}^{+}$ that estimates the spatial distribution of the dipole-wise power like the rate between the neural activity and true power of the simulated sources. As a consequence, the index ε_s measures the effort needed to transform the estimated power distribution into the actual distribution by transporting the probability mass [35]. Thus, the lower the ε_s value, the better the performed reconstruction.

Temporal Accuracy Index, $\varepsilon_t{\in}\mathbb{R}[0,1]$, that quantifies the correlation between each simulated time series and its respective reconstructed signal for all dipoles. For each simulated source, the maximum correlation is computed across all dipoles and spatial orientations. Also, the maximum values are averaged across the simulated sources to give an average maximum correlation. As a result, a higher value of ε_t implies a better reconstruction performed in the time domain.

C. Real-world EEG data of emotion analysis

In this study, the EEG data used were obtained from the publicly available reservoir devoted to emotion

analysis using physiological signals (DEAP) [36]. Thirty-two healthy participants (50% females and 50% males on average aging 26.9 years) were recruited and consented to participate in the study. Collecting EEG recordings by the BIOSEMI ActiveTwo system, data were acquired at a sampling rate $512\,Hz$, placing electrodes on the surface scalp and according to the International $10-20$ system. The applied pre-processing included the following steps: common referencing, down-sampling to $128\,Hz$, high-pass filtering from $4\,Hz$, and eye-blink artifact removal using independent component analysis.

Although the DEAP participants rated the felt emotion employing a discrete 9-point scale, the classification task had been relaxed by binarizing all subject's scores at the scale midpoint (i.e., at 5-point level), resulting in the basic setting of bi-class patterns (particularly, low versus high as pictured in Fig. 3). For each emotion classification task, therefore, we reflect the bi-class affective conditions: Valence (negative versus positive), Arousal (passive-active), Dominance (dominated-dominant), and Liking (dislike-like).

In this task of emotion analysis, we consider the influence of the following two main procedures:

Source space reconstruction: This procedure is evaluated using each one of the considered neural reconstruction solutions, for which the parameters (i.e., spatial basis), regularization parameter tuning, and implementation of the volume conductor model (i.e., the lead field matrix) are accomplished as in the above-simulated dataset set-up. So, we verify the performed source reconstruction, according to the certainty achieved to differentiate the related bi-class emotions. Using a two-sided pairwise Student *t*-test, we estimate the significant differences in brain activity (dipole-wise source power) for each trial. Thus, the *t*-score maps of brain areas, obtained for each emotion with absolute values greater than 2.0244 (i.e., significance levels $p<$ 0.05 uncorrected), are associated with the regions having a differentiable neural activity between either affective condition: low or high.

IV. Results

A. Performed reconstruction for simulated data

As seen in Fig. 4 that displays the performed quality of spatial reconstruction, the cases when the analyzed EEG inverse solutions do not include any temporal information (like LASSO, S-FLEX, and MSP) yield the lowest spatial accuracy (that is, higher ϵ_s values) within the whole tested SNR range, getting worse as the neural dynamic complexity increases. Hence, the lack of information about temporal EEG dynamics certainly degrades the spatial localization accuracy of active brain areas. Besides, the FUSION solution that does not account for any spatial structure produces a very low spatial accuracy, indicating that the only inclusion of the temporal dynamics is not enough for properly describing the spatial patterns of neural activity. In contrast, the spatial performance can be enhanced if a trade-off between spatial and temporal patterns is incorporated like in the solutions DSC(90:30), DSC(30:90), and the balanced compromise DSC(90:90) that achieves the best spatial performance.

In the same way, the quality of temporal reconstruction behaves. So, the solutions that do not include any temporal constraints perform the worst (like in LASSO, S-FLEX, and MSP), reaching the lowest correlation values. Moreover, the single inclusion of a strong temporal constraint does not lead to a better quality than the solutions perform without temporal constraints. Once again, the DSC proposal that includes a space-time trade-off allows enhancing the quality of temporal reconstruction as it is the case for the ratios (90:30), (90:90), and (30:90). However, when the temporal term weighs more than the spatial one, like in DSC(30:90), a higher correlation value is obtained.

Further, for providing an objective comparison we employ a paired $t-$test between each pair of the tested ESI solutions, assuming as null hypothesis that there are no significant differences between the compared methods concerning both, the spatial accuracy index ϵ_s (see Fig. 6), and the temporal accuracy index ϵ_t (see Fig. 6). Otherwise, the alternative hypothesis affirms, in the former case (spatial performance), that the mean ϵ_s value of the method in the row is confidently lower that the mean ϵ_s value of the method in the column. Conversely, for the temporal accuracy index, the alternative hypothesis affirms that the mean ϵ_t value of the method in the row is significantly greater than the mean ϵ_t value belonging to the method in the column. Moreover, gray and black blocks represent that the null hypothesis is rejected at significance levels $p = 0.05$ and $p = 0.01$, respectively.

Both the spatial accuracy index ϵ_s Fig. 6, and the temporal accuracy index Fig. 7 confirm that as long as the EEG temporal dynamics increases, i.e., the number of active sources increases, methods that do not include such dynamic information achieve lower results than methods that merge both spatial and temporal constraints. As a result, DSC(90:90) and DSC(30:90) obtain, in most of the studied cases, ϵ_s values significantly lower than the remaining methods.

Grounded on the obtained-above results, we state that as the analyzed data display a more nonstationary behavior the accurate localization of the brain activity generators become more difficult. In this regard, DSC can be adjusted through the spatial-to-temporal regularization ratio (i.e., λ_s:λ_t) to emphasize either the spatial or temporal reconstruction, depending on the requirements of accuracy available for the specific data in hand.

B. Performed quality of emotion-related neural activity

The performed differences in dipole-wise power between the high and low affective conditions are calculated for the DSC(30:90) solution since it reaches the best accuracy of neural reconstruction performed for the simulated EEG data. Fig. 8 displays some examples of *t*-score maps, showing the most significant differences (areas in the dark color) and leading to the following findings:

- *Valence emotion*. In this case, the identified brain regions with the most significant differences are close to the default-mode network. For the positive valence, some differences (colored in dark red) are noted in the medial frontal and prefrontal cortex that is associated with pleasant and unpleasant emotions. Also, the posterior cingulate gyrus area that is involved in emotional processing shows marked differentiation in activity. These findings are agreeing with results reported in [37].

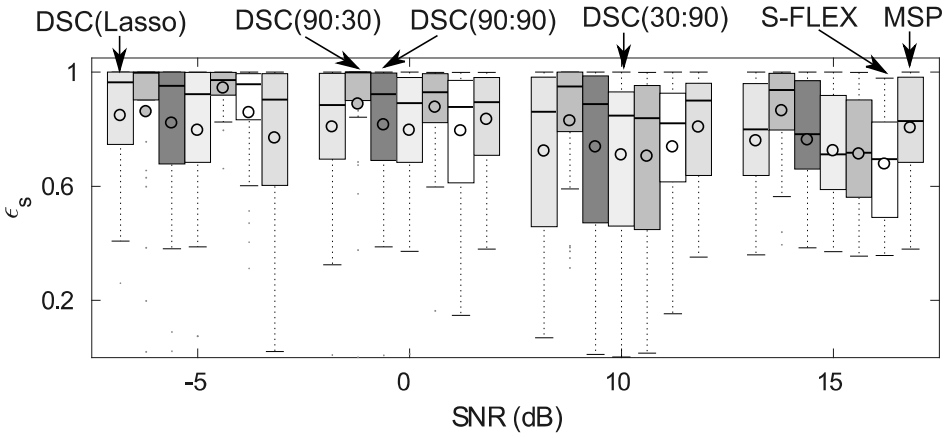

(a) One active source

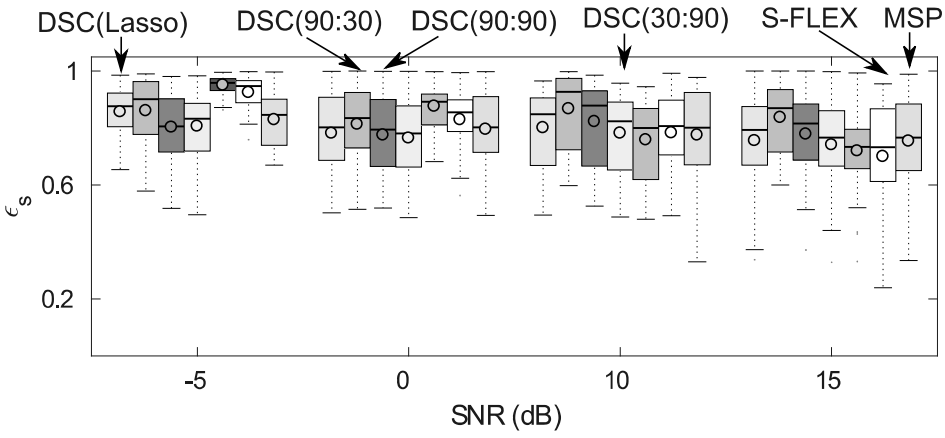

(b) Three active sources

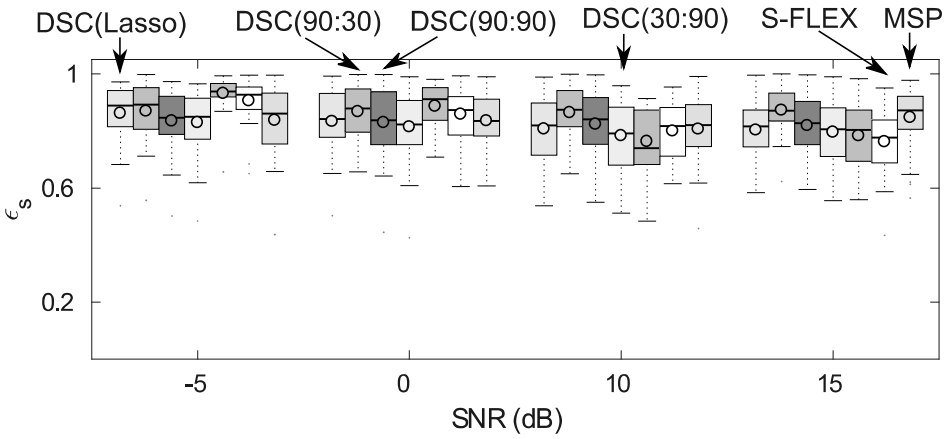

(c) Five active sources

Fig. 4. Spatial reconstruction accuracy according to the *Earth-Mover's Distance* ε_s in the first experiment for the following mappings methods: DSC(Lasso), DSC(90 : 30), DSC(90 : 90), DSC(30 : 90), DSC(Fusion), S-FLEX, MSP.

- *Arousal emotion*. Mainly, the regions with the important differences relate to the high arousal rates like in the ventral anterior cingulate gyrus that is commonly associated with the sexual arousal produced by visual stimuli in males [38]. Also, the temporal pole (linked with the visual processing of emotional images [39]) holds a high activity. For the passive activity (i.e., lower arousal rates), the notable differences are in the posterior cingulate gyrus associated with the process of emotional semantic information and actions of passively listening to different sentences as suggested in [40]. Likewise, several areas regarding visual stimuli processing are active, for instance, the middle occipital gyrus.
- *Dominance emotion*. As noted in [41] for high values (dominant), the superior parietal lobule, which regards the processing emotions and self-reflections during decision making, reveals a high activity, as well as in the posterior cingulate gyrus linked with fear conditioning and evaluative judgment [42], [43]. For low dominance (dominated), a high activity is located in part of the prefrontal cortex associated with the pleasant and unpleasant emotions.
- *Liking emotion*. In the case of the subject dislikes videos, the active regions are the posterior cingulate gyrus (related to evaluative judgment) and the inferior

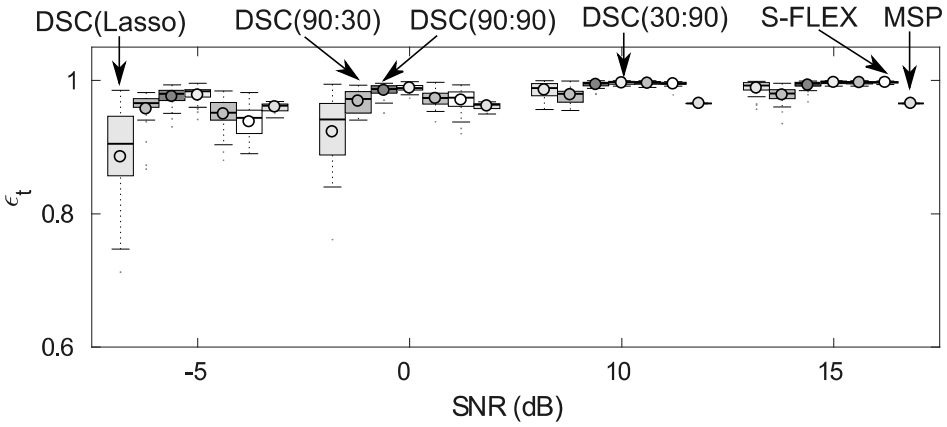

(a) One active source

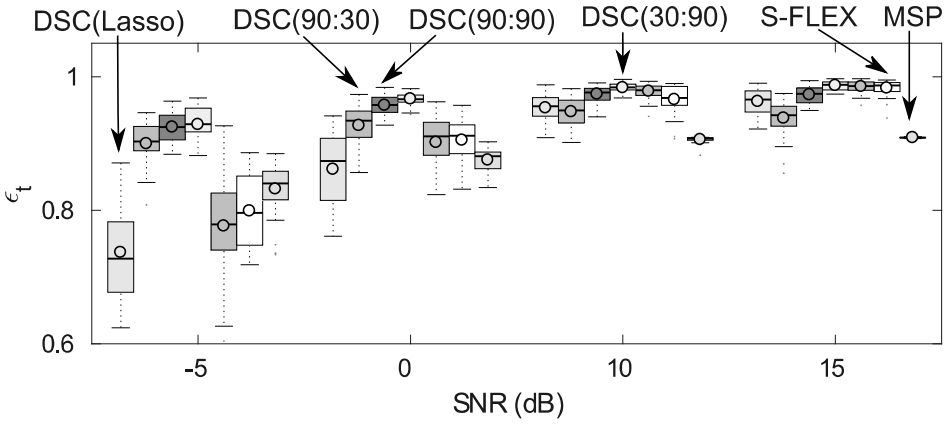

(b) Three active sources

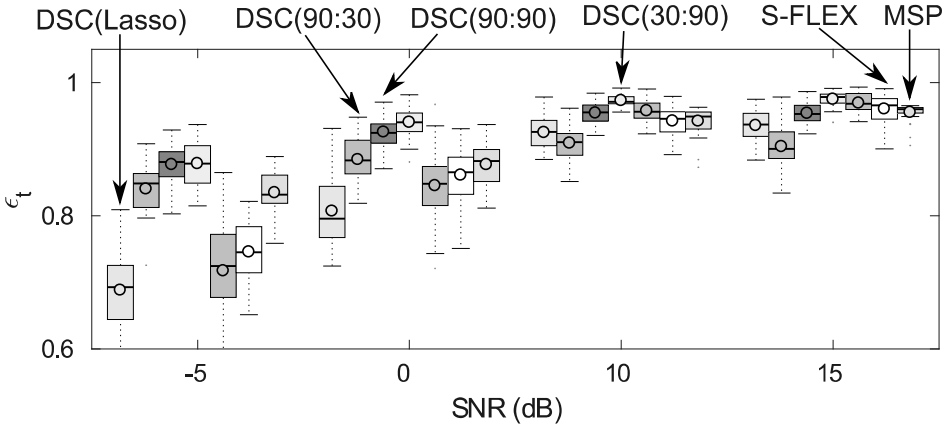

(c) Five active sources

Fig. 5. Temporal reconstruction accuracy according to the *maximum correlation* ε_t in the first experiment for the following mappings methods: DSC(Lasso), DSC(90 : 30), DSC(90 : 90), DSC(30 : 90), DSC(Fusion), S-FLEX, MSP.

parietal lobule (associated with retrieval of unpleasant experiences [44]). In the opposite situation of liking videos, the active areas associate with music enjoyment as the inferior frontal gyrus [45].

Regardless of the examined emotion, there is an active brain area close to the secondary visual cortex. The finding is explained because this area is highly associated with the response to emotion/attention in visual processing [46].

V. Discussion

Aiming to enhance the spatio-temporal resolution, we propose a regularized method for neural activity reconstruction that explicitly includes both (space and time) constraints on the M/EEG inverse problem solution. The main goal is to reach a suitable trade-off between the corresponding space and time resolutions, allowing to more accurately estimate the active sources that better encode a high non-stationary behavior of brain activity. From the above-obtained results, however, the following findings are worth mentioning:

We foster the enhancement of the spatial resolution by representing the brain activity as a sum of a small number of space basis functions, describing a set of smooth localized patches that adequately represents all potentially active brain regions. To this, we incorporate a spatial constraint that is expressed in terms of the L_1-norm so that we promote the

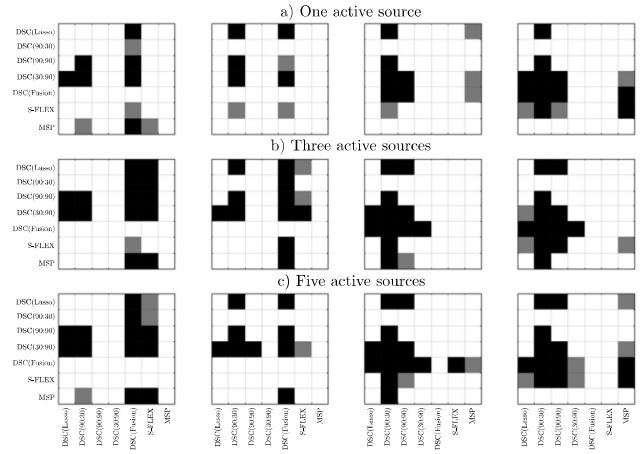

Fig. 6. Paired $t-$test comparing the tested ESI solutions with the spatial accuracy index ϵ_s, for one, three, and five active sources, and for the different SNR values, namely, from left to right at each row: $-5dB$, $0dB$, $10dB$, and $15dB$. In the $t-$ test alternative hypothesis, the method in the column is assumed to have a significantly lower ϵ_s mean value.

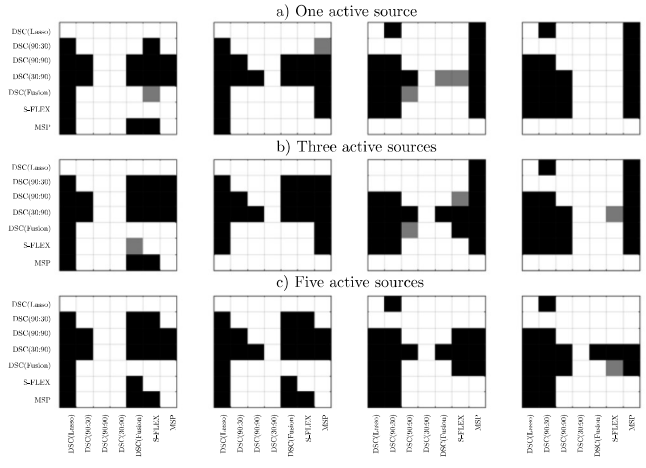

Fig. 7. Paired $t-$test comparing the tested ESI solutions with the temporal accuracy index ϵ_t, for one, three and five active sources, and for the different SNR values, namely, from left to right at each row: $-5dB$, $0dB$, $10dB$, and $15dB$. In the $t-$ test alternative hypothesis, the method in the column is assumed to have a significantly greater ϵ_t mean value.

solution to be sparse, making the estimated brain activity be represented mainly by a set of localized sources. Thus, the influence of the spatial constraint on the estimated solution is ruled by increasing or decreasing the regularization parameter λ_s. Besides, we include a temporal regularization term that encourages the inverse problem solution to improve the temporal accuracy of the accomplished neural activity reconstruction. As a result, this term penalizes the difference between consecutive time samples, leading to a smooth solution over time.

In order to obtain an enhanced resolution, the inclusion of a single constraint, either spatial or temporal, within the proposed DSC solution is clearly nor enough, degrading the solution performance as accomplished by the asymptotic cases (λ_s=0, or λ_t=0). Rather, we notably improve the reconstruction quality when an adequate compromise between both regularization parameters is established. Moreover, the DSC solution enables adjusting the spatio-temporal ratio, depending on dynamics of available EEG data.

Therefore, one of the most crucial stages is the regularization parameter tuning of DSC solution. In this regard, we employ the *Sparsest possible solution* that does not demand an exhaustive search nor an exhaustive computational cost like other approaches, which commonly carry out the calculation of several solutions with different parameters tuned just by a single EEG recording.

VI. Conclusions

In this work, we introduce a method that imposes physiologically motivated spatio-temporal constraints on a Dynamic Sparse Coding for improving the quality of brain activity reconstruction and localization. The proposed method provides a trade-off between the imposed spatial and temporal constraints through the regularization parameters, enhancing the estimation of non-stationary neural activity.

For the sake of validation of the reconstructed neural activity in real scenarios, we carry out an analysis of the generators of emotion-related brain activity, showing that most active sources originate in cortical areas involved in visual and attention processes, as well as in regions involved in emotional processing. This finding stands in line with the literature. As a result, the proposed DSC-based solution improves previous characterizations of M/EEG source activity, particularly, when dealing with strong temporal dynamics.

As the future work, we plan to improve the spatial resolution of our method, including the fMRI-based spatial basis. Also, we plan to include time-frequency based constraints towards obtaining more accurate source reconstruction in practice.

References

[1] M. Koppert, S. Kalitzin, D. Velis, F. L. da Silva, and M. Viergever, "Dynamics of collective multi-stability in models of distributed neuronal systems," *International Journal of Neural Systems*, vol. 24, no. 2, p. 1430004, 2014.

[2] X. Lei, T. Wu, and P. A. Valdes-Sosa, "Incorporating priors for eeg source imaging and connectivity analysis," *Frontiers in neuroscience*, vol. 9, 2015.

[3] J.-M. Schoffelen and J. Gross, "Source connectivity analysis with meg and eeg," *Human brain mapping*, vol. 30, no. 6, pp. 1857–1865, 2009.

[4] R. Sukanesh and R. Harikumar, "A comparison of genetic algorithm & neural network (MLP) in patient specific classification of epilepsy risk levels from EEG signals," *Engineering Letters*, vol. 14, no. 1, pp. 96–104, 2007.

[5] ——, "A patient specific neural networks (MLP) for optimization of fuzzy outputs in classification of epilepsy risk levels from EEG signals," *Engineering Letters*, vol. 13, no. 2, pp. 50–56, 2006.

[6] ——, "Diagnosis and classification of epilepsy risk levels from eeg signals using fuzzy aggregation techniques," *Engineering Letters*, vol. 14, no. 1, pp. 90–95, 2007.

[7] M. J. Barton, P. a. Robinson, S. Kumar, A. Galka, H. F. Durrant-Whyte, J. Guivant, and T. Ozaki, "Evaluating the performance of kalman-filter-based EEG source localization." *IEEE transactions on bio-medical engineering*, vol. 56, no. 1, pp. 122–36, Jan. 2009.

[8] R. Huster, S. Debener, T. Eichele, and C. Herrmann, "Methods for simultaneous eeg-fmri: An introductory review," *Journal of Neuroscience*, vol. 18, no. 32, pp. 6053–6060, may 2012.

[9] B. Babadi, G. Obregon-Henao, C. Lamus, M. S. Hämäläinen, E. N. Brown, and P. L. Purdon, "A subspace pursuit-based iterative greedy hierarchical solution to the neuromagnetic inverse problem," *NeuroImage*, vol. 87, pp. 427–443, 2014.

[10] R. D. Pascual-Marqui, "Review of methods for solving the EEG inverse problem," *International journal of bioelectromagnetism*, vol. 1, no. 1, pp. 75–86, 1999.

[11] R. D. Pascual-Marqui, C. M. Michel, and D. Lehmann, "Low resolution electromagnetic tomography: a new method for localizing electrical activity in the brain," *International Journal of psychophysiology*, vol. 18, no. 1, pp. 49–65, 1994.

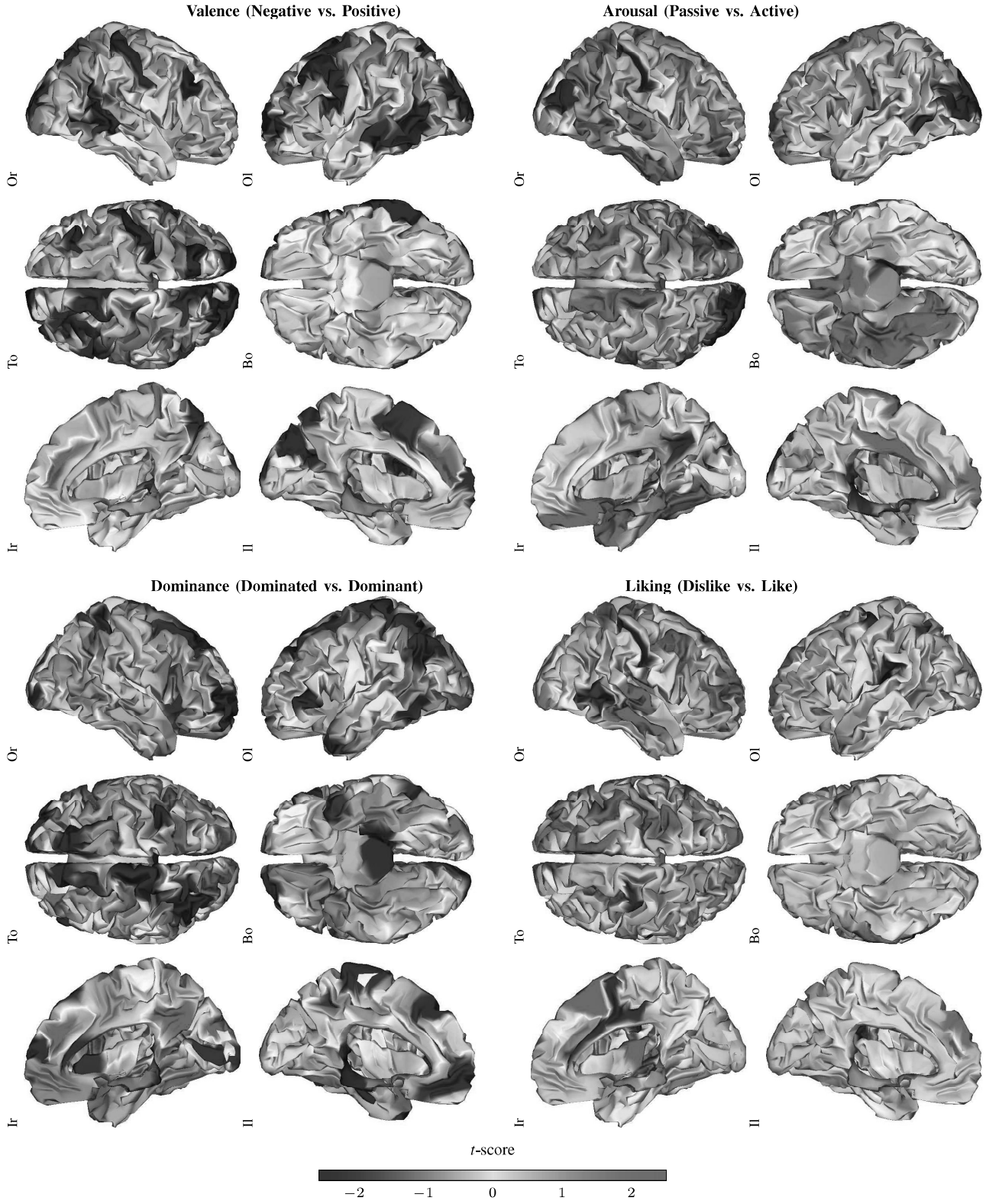

Fig. 8. Examples of *t*-score maps computed for differences in dipole-wise power between high/low valence (sub12), high/low arousal (sub 29), high/low dominance (sub 15), and high/low liking (sub 20). Views: Outside right (Or), Outside left (Ol), Top (To), Bottom (Bo), Inside right (Ir) and Inside left (Il).

[12] R. Grech, T. Cassar, J. Muscat, K. Camilleri, S. Fabri, M. Zervakis, P. Xanthopoulos, V. Sakkalis, and B. Vanrumste, "Review on solving the inverse problem in EEG source analysis," *Journal of NeuroEngineering and Rehabilitation*, vol. 5, no. 25, pp. 792 –800, june 2008.

[13] M. Vega-Hernndez, E. Martnez-Montez, J. M. Snchez-Bornot, and A. Lage-Castellanos, "Penalized least squares methods for solving the EEG inverse problem," *Statistica Sinica*, vol. 18, no. 18, pp. 1535–1551, 2008.

[14] K. Friston, L. Harrison, J. Daunizeau, S. Kiebel, C. Phillips, N. Trujillo-Barreto, R. Henson, G. Flandin, and J. Mattout, "Multiple sparse priors for the m/eeg inverse problem," *NeuroImage*, vol. 39, no. 3, pp. 1104–1120, 2008.

[15] S. Haufe, R. Tomioka, T. Dickhaus, C. Sannelli, B. Blankertz, G. Nolte, and K.-R. Muller, "Large-scale eeg/meg source localization with spatial flexibility," *NeuroImage*, vol. 54, no. 2, pp. 851 – 859, 2011.

[16] S. Kalitzin, M. Koppert, G. Petkov, and F. L. da Silva, "Multiple oscillatory states in models of collective neuronal dynamics," *International Journal of Neural Systems*, vol. 24, no. 6, p. 1450020,

2014.
[17] K. Liu, Z. L. Yu, W. Wu, Z. Gu, and Y. Li, "Straps: A fully data-driven spatio-temporally regularized algorithm for M/EEG patch source imaging," *International Journal of Neural Systems*, vol. 25, no. 04, p. 1550016, 2015.
[18] A. Bolstad, B. Van Veen, and R. Nowak, "Space–time event sparse penalization for magneto-/electroencephalography," *NeuroImage*, vol. 46, no. 4, pp. 1066–1081, 2009.
[19] P. Munoz-Gutiérrez, E. Giraldo, M. Bueno-López, and M. Molinas, "Localization of active brain sources from EEG signals using empirical mode decomposition: A comparative study," *Frontiers in Integrative Neuroscience*, vol. 12, no. 1, pp. 1–13, 2018.
[20] P. Belardinelli, E. Ortiz, G. Barnes, U. Noppeney, and H. Preissl, "Source reconstruction accuracy of MEG and EEG Bayesian inversion approaches," *PLoS ONE*, vol. 7, no. 12, p. e51985, 12 2012.
[21] M. W. Woolrich, A. Baker, H. Luckhoo, H. Mohseni, G. Barnes, M. Brookes, and I. Rezek, "Dynamic state allocation for MEG source reconstruction," *NeuroImage*, vol. 77, pp. 77 – 92, 2013.
[22] P. A. Valdés-Sosa, M. Vega-Hernández, J. M. Sánchez-Bornot, E. Martínez-Montes, and M. A. Bobes, "Eeg source imaging with spatio-temporal tomographic nonnegative independent component analysis," *Human brain mapping*, vol. 30, no. 6, pp. 1898–1910, 2009.
[23] A. Gramfort, D. Strohmeier, J. Haueisen, M. Hmlinen, and M. Kowalski, "Time-frequency mixed-norm estimates: Sparse m/eeg imaging with non-stationary source activations," *NeuroImage*, vol. 70, no. 0, pp. 410 – 422, 2013.
[24] F. Costa, H. Batatia, T. Oberlin, C. D'Giano, and J.-Y. Tourneret, "Bayesian eeg source localization using a structured sparsity prior," *NeuroImage*, 2016.
[25] J. Daunizeau, J. Mattout, D. Clonda, B. Goulard, H. Benali, and J.-M. Lina, "Bayesian spatio-temporal approach for eeg source reconstruction: conciliating ecd and distributed models," *IEEE Transactions on Biomedical Engineering*, vol. 53, no. 3, pp. 503–516, 2006.
[26] M. Fukushima, O. Yamashita, A. Kanemura, S. Ishii, M. Kawato, and M.-a. Sato, "A state-space modeling approach for localization of focal current sources from meg," *IEEE Transactions on Biomedical Engineering*, vol. 59, no. 6, pp. 1561–1571, 2012.
[27] S. Baillet, J. C. Mosher, and R. M. Leahy, "Electromagnetic Brain Mapping," *Signal Processing Magazine, IEEE*, vol. 18, no. November, pp. 14 –30, 2001.
[28] S. Castaño-Candamil, J. Höhne, J.-D. Martínez-Vargas, X.-W. An, G. Castellanos-Domínguez, and S. Haufe, "Solving the eeg inverse problem based on space–time–frequency structured sparsity constraints," *NeuroImage*, vol. 118, pp. 598–612, 2015.
[29] P. Käufl, A. Valentine, R. De Wit, and J. Trampert, "Solving probabilistic inverse problems rapidly with prior samples," *Geophysical Journal International*, pp. ggw108+, Mar. 2016.
[30] G. E, J. Martinez-Vargas, and G. Castellanos-Dominguez, "Reconstruction of neural activity from EEG data using dynamic spatio-temporal constraints," *International Journal of Neural Systems*, vol. 26, no. 7, pp. 16 500 261–165 002 615, 2016.
[31] X. Chen, Q. Lin, S. Kim, J. G. Carbonell, and E. P. Xing, "Smoothing proximal gradient method for general structured sparse regression," *Ann. Appl. Stat.*, vol. 6, no. 2, pp. 719–752, 06 2012. [Online]. Available: http://dx.doi.org/10.1214/11-AOAS514
[32] R. Chalasani and J. C. Principe, "Dynamic sparse coding with smoothing proximal gradient method," in *2014 IEEE International Conference on Acoustics, Speech and Signal Processing (ICASSP)*. IEEE, 2014, pp. 7188–7192.
[33] Y. Nesterov, "Smooth minimization of non-smooth functions," *Mathematical Programming*, vol. 103, no. 1, pp. 127–152, 2005.
[34] T. R. Mullen, C. A. Kothe, Y. M. Chi, A. Ojeda, T. Kerth, S. Makeig, T.-P. Jung, and G. Cauwenberghs, "Real-time neuroimaging and cognitive monitoring using wearable dry eeg," *Biomedical Engineering, IEEE Transactions on*, vol. 62, no. 11, pp. 2553–2567, 2015.
[35] S. Haufe, V. V. Nikulin, A. Ziehe, K.-R. Mller, and G. Nolte, "Combining sparsity and rotational invariance in eeg/meg source reconstruction," *NeuroImage*, vol. 42, no. 2, pp. 726 – 738, 2008.
[36] S. Koelstra, C. Muhl, M. Soleymani, J.-S. Lee, A. Yazdani, T. Ebrahimi, T. Pun, A. Nijholt, and I. Patras, "Deap: A database for emotion analysis ;using physiological signals," *Affective Computing, IEEE Transactions on*, vol. 3, no. 1, pp. 18–31, Jan 2012.
[37] L. Kuchinke, A. M. Jacobs, C. Grubich, M. L.-H. Vo, M. Conrad, and M. Herrmann, "Incidental effects of emotional valence in single word processing: an fmri study," *Neuroimage*, vol. 28, no. 4, pp. 1022–1032, 2005.
[38] S. Kim, D. Sohn, Y. Cho, W. Yang, K. Lee, R. Juh, K. Ahn, Y. Chung, S. Han, K. Lee *et al.*, "Brain activation by visual erotic stimuli in healthy middle aged males," *International journal of impotence research*, vol. 18, no. 5, pp. 452–457, 2006.
[39] T. Tsukiura, M. Namiki, T. Fujii, and T. Iijima, "Time-dependent neural activations related to recognition of people's names in emotional and neutral face-name associative learning:: an fmri study," *Neuroimage*, vol. 20, no. 2, pp. 784–794, 2003.
[40] R. S. Patel, F. D. Bowman, and J. K. Rilling, "Determining hierarchical functional networks from auditory stimuli fmri," *Human brain mapping*, vol. 27, no. 5, pp. 462–470, 2006.
[41] M. Deppe, W. Schwindt, H. Kugel, H. Plassmann, and P. Kenning, "Nonlinear responses within the medial prefrontal cortex reveal when specific implicit information influences economic decision making," *Journal of Neuroimaging*, vol. 15, no. 2, pp. 171–182, 2005.
[42] S. Zysset, O. Huber, E. Ferstl, and D. Y. von Cramon, "The anterior frontomedian cortex and evaluative judgment: an fmri study," *Neuroimage*, vol. 15, no. 4, pp. 983–991, 2002.
[43] T. K. Doronbekov, H. Tokunaga, Y. Ikejiri, H. Kazui, N. Hatta, Y. Masaki, A. Ogino, N. Miyoshi, N. Oku, T. Nishikawa *et al.*, "Neural basis of fear conditioning induced by video clip: positron emission tomography study," *Psychiatry and clinical neurosciences*, vol. 59, no. 2, pp. 155–162, 2005.
[44] T. Ushida, T. Ikemoto, S. Tanaka, J. Shinozaki, S. Taniguchi, Y. Murata, M. McLaughlin, Y.-C. P. Arai, and Y. Tamura, "Virtual needle pain stimuli activates cortical representation of emotions in normal volunteers," *Neuroscience letters*, vol. 439, no. 1, pp. 7–12, 2008.
[45] S. Koelsch, T. Fritz, K. Müller, A. D. Friederici *et al.*, "Investigating emotion with music: an fmri study," *Human brain mapping*, vol. 27, no. 3, pp. 239–250, 2006.
[46] R. D. Lane, E. M. Reiman, M. M. Bradley, P. J. Lang, G. L. Ahern, R. J. Davidson, and G. E. Schwartz, "Neuroanatomical correlates of pleasant and unpleasant emotion," *Neuropsychologia*, vol. 35, no. 11, pp. 1437–1444, 1997.